

Article

Microstructural Investigations of VO₂ Thermo-chromic Thin Films Grown by Pulsed Laser Deposition for Smart Windows Applications

Ayushi Rai ¹, Nicusor Iacob ², Aurel Leca ², Claudiu Locovei ², Victor Kuncser ², Cristian N. Mihailescu ³ and Andreas Delimitis ^{1,*}

¹ Department of Mechanical and Structural Engineering and Materials Science, University of Stavanger, N-4036 Stavanger, Norway

² National Institute of Materials Physics, Atomistilor 405A, RO 077125 Magurele, Romania

³ National Institute for Laser, Plasma and Radiation Physics, Atomistilor 409, RO 077125 Magurele, Romania

* Correspondence: andreas.delimitis@uis.no; Tel.: +47-518-32757

Abstract: The structural properties of VO₂ thin films, grown on either LSAT or Si substrates by pulsed laser deposition (PLD), are elucidated by means of transmission electron microscopy (TEM) methods. The TEM observations confirmed the successful growth of VO₂ by PLD in variable thicknesses, by optimizing the O₂ partial pressure and growth temperature. The films adopt a columnar polycrystalline morphology with narrow columns, up to the film thickness height. Four VO₂ polymorphs have been detected by electron diffraction and high-resolution TEM (HRTEM) analysis, with M1 being by far the most abundant phase. Post-experimental strain measurements in HRTEM images have revealed that the actual residual strain is minimized due to the columnar morphology of the VO₂ grains, as well as intrinsic oxide layers in the VO₂/Si epitaxy. The TEM outcomes confirmed the complementary electrical and magnetic measurements in the films, where a transition from a monoclinic M1 to a rutile VO₂ R phase has been identified, influenced by the initial percentage of phases in thick VO₂ films.

Keywords: thermo-chromic VO₂; TEM/HRTEM; GPA; electron diffraction; structural defects; PLD; smart windows; electrical resistivity



Citation: Rai, A.; Iacob, N.; Leca, A.; Locovei, C.; Kuncser, V.; Mihailescu, C.N.; Delimitis, A. Microstructural Investigations of VO₂ Thermo-chromic Thin Films Grown by Pulsed Laser Deposition for Smart Windows Applications. *Inorganics* **2022**, *10*, 220. <https://doi.org/10.3390/inorganics10120220>

Academic Editors: Duncan H. Gregory, Wolfgang Linert, Richard Dronskowski, Vladimir Arion, Claudio Pettinari and Torben R. Jensen

Received: 31 October 2022

Accepted: 22 November 2022

Published: 24 November 2022

Publisher's Note: MDPI stays neutral with regard to jurisdictional claims in published maps and institutional affiliations.



Copyright: © 2022 by the authors. Licensee MDPI, Basel, Switzerland. This article is an open access article distributed under the terms and conditions of the Creative Commons Attribution (CC BY) license (<https://creativecommons.org/licenses/by/4.0/>).

1. Introduction

The requirement to maintain energy comfort in buildings accounts for approximately 40% of the total energy consumption. More than 50% of the building energy is consumed in heating, air conditioning, and ventilation [1–6]. One way to minimize this is to replace conventional windows with smart ones, which adjust heat (infrared) transmittance by controlling the solar irradiation and enable buildings to keep a temperature without any need for cooling or heating [7–13]. This approach has become an important topic of research in recent times.

Thermo-chromic materials are capable of changing their optical properties by temperature variations as an external stimulation. Thermo-chromics have been used as coatings on windows for energy saving applications due to their luminous transmittance and solar modulation ability [14–16]. In order to use thin film coatings for practical applications, there are several properties that need to be controlled. The critical or phase transition temperature, T_c , must be decreased to around room temperature, while maintaining a good visible light transmittance (nearly 60%). A satisfactory electrical and optical performance is inevitably correlated with the microstructural changes induced in thin film coatings [17].

Vanadium dioxide (VO₂) is a transition metal oxide with unique properties due to its reversible phase transition temperature ($T_c = 68$ °C). Below this temperature, VO₂ behaves as an insulator with a monoclinic structure (M1 phase). However, above T_c , it

undergoes a lattice distortion to a rutile-type tetragonal structure (R phase), exhibiting metallic behavior. Thus, above T_c , VO_2 reflects a large amount of solar radiation which makes it a good candidate for application in thermochromic smart windows [18–22]. In recent times, very promising thermochromic performances of the VO_2 -based coatings have been reported [23]. Kolenatý et al. reported a thermochromic $\text{ZrO}_2/\text{V}_{0.982}\text{W}_{0.018}\text{O}_2/\text{ZrO}_2$ multilayer coating with a low transition temperature of 21 °C, which was deposited by low-temperature magnetron sputtering [24]. Malarde et al. reported VO_2 thin films prepared using atmospheric-pressure chemical vapor deposition, showing $\Delta T_{\text{sol}} = 12\%$ [25].

The defect concentration and strain affect the electrical and optical properties of VO_2 thin films. It is well known that phase transition in VO_2 is strongly influenced by the strain along tetragonal axes [18]. The nature of the microstructure such as the concentration of defects, nature of grain boundaries, and grain size all influence the MIT (metal-to-insulator transition) sharpness, amplitude, and thermal hysteresis [19]. A narrow hysteresis loop shows a fast phase transition which is desirable in this case.

The modulation of the critical temperature of VO_2 to room temperature is essential for its practical application in smart windows. Many attempts have been made to do so by doping, applying external electric and magnetic field, strain, etc. However, the thermochromic performance of VO_2 has not been optimized yet and often decreases with these strategies [26,27]. Therefore, attempts towards understanding the correlation between the structural features of the films and the involved MIT are of crucial importance for their proper engineering and optimization with respect to thermochromic applications.

In this work, we report on the structural features of VO_2 thermochromic thin films grown on LSAT ($\text{La}_{0.18}\text{Sr}_{0.82}\text{Al}_{0.59}\text{Ta}_{0.41}\text{O}_3$) or Si substrates by pulsed laser deposition (PLD). Although VO_2 thin films have been deposited on various substrates thus far, a comparative study between the two substrates, LSAT and Si, has not been performed, to the extent of our knowledge, up to now. The substrates were chosen as alternatives to quartz, in order to replicate some of the substrates used for growing VO_2 of different texture and morphology, but also to resemble the usual transparent glass. The aim of the study is to investigate the role of different crystalline phases, as well as the overall film morphology in the MIT behavior. Therefore, only those samples obtained under preparation conditions (including the type of substrate and substrate temperature) leading to finite amounts of the most usual VO_2 phases but with a predominant and comparable M1-type phase have been selected. PLD has been already successfully established as a growth technique for crystalline VO_2 films [28,29], due to providing precise control of oxygen partial pressure for stoichiometric components and a high temperature that contributes to good crystallinity [30,31]. Since a mixture of VO_2 phases was observed by X-ray diffraction, which are difficult to quantify, transmission electron microscopy (TEM) was performed for a thorough investigation of the film's structural aspects. The general morphology, film thickness, interfacial and surface roughness, crystallographic orientation, and epitaxial relationship of films and substrates were deduced. Electrical resistance and magnetic measurements were further conducted to investigate the electronic and phase-transition properties of VO_2 thin films, proving finally that the MIT is not simply solely related to the stabilization of the M1 phase of the VO_2 film below room temperature (RT). Hence, it was shown that an unstable M1-type phase is required, and in the conditions of marginal residual strains, as in the reported samples, only a very low fraction of the initial M1 phase is transformed to the R phase.

2. Experimental Methods

Pulsed laser deposition (PLD) was employed to grow epitaxial VO_2 on (001) LSAT or (001) Si substrates. All thin films were grown using a KrF*excimer laser as an ablation source (COMPex PRO $\lambda = 248$ nm, $T_{\text{FWHM}} = 25$ ns). The PLD process was conducted under ultra-high vacuum conditions, and the target was ablated at 45° with respect to the focused laser beam keeping parallel with the substrate. The target was continuously rotated in the target carousel to achieve uniform deposition. The oxygen partial pressure was maintained at 10^{-2} mbar while the substrate temperature was 500 °C. The thickness of the film was

controlled by the number of pulses which varied from 5000 to 100,000. The films involved in this study are denoted as S1, S2, and S3, possessing 100,000, 20,000, and 50,000 pulses and grown on LSAT (S1) and Si (S2 and S3) substrates, respectively.

Microstructural studies were performed on a JEOL 2100 electron microscope operating at 200 kV, with a point resolution of 0.23 nm and an electron nanoprobe size down to 1 nm, for performing diffraction studies and chemical analysis at the nanoscale. Cross-sectional TEM samples were prepared by mechanical polishing and precision Ar⁺ milling at low energies.

The magnetic behavior of the films was investigated by performing magnetization measurements versus temperature under an applied field of 300 Oe, by using the most sensitive reciprocal space option (RSO) of a superconducting quantum interference device (SQUID), MPMS-7T from Quantum Design. Small rectangular pieces (3 mm × 3 mm) of VO₂ films deposited on either LSAT or Si substrates were cut in this respect, and the field was applied parallel to the film. The contribution of the substrate has been subtracted by reference measurements.

Electron transport measurements were performed using the ACT option of a physical property measurement system, PPMS-14T from Quantum Design. The four points method was used with in-line contacts made on the films on the LSAT and Si substrates, cut as rectangular pieces of 8 mm × 2.5 mm. The inner electrodes collecting voltage were separated by 2 mm. An AC current of 0.2 mA at a frequency of 17 Hz was applied on the external electrodes, and the resistance (in Ohm) was registered over the temperature interval from 250 to 360 K.

3. Result and Discussion

Qualitatively structural analysis by X-ray diffraction (XRD) in the samples revealed that several phases of VO₂ are simultaneously present, due to the multiplicity of phases in the VO₂ system. Their relative percentages, as well as the low thickness of the VO₂ thin films, render it difficult to clearly distinguish the phases by XRD. Therefore, transmission electron microscopy (TEM) was subsequently employed for qualitative and quantitative structural phase identification.

A cross-sectional image of the S1 VO₂ thin film grown on the LSAT substrate is shown in Figure 1a. The TEM investigations confirmed that the growth of the film by PLD was accomplished, and an overall coverage of VO₂ on top of LSAT was achieved. The total thickness of this film was 720 nm, for 100,000 pulses. In terms of morphology, there was columnar growth of VO₂, with a column width of around 170 nm, which is a common feature in the case of deposition of VO₂ thin films on various substrates [32,33]. The selected area diffraction (SAD) pattern of S1 in Figure 1b was obtained by an area at the VO₂/LSAT interface and shows reflections by both the substrate and film. The LSAT substrate is viewed along its [001] zone axis, whereas the VO₂ film has a polycrystalline structure [29,34]. Furthermore, the SAD experiments revealed the co-existence of various VO₂ polymorphs in the film, such as VO₂ M1, VO₂ B, VO₂ A, and VO₂ R. The structural parameters of these polymorphs are outlined in Table 1. In addition, the arcing of the VO₂ spots and their alignment with the main ones of LSAT indicated that there is a tendency towards a structural relationship between the various VO₂ phases in the thin film and the LSAT substrate. In more detail, this preferential orientation, with regards to the substrate can be summarized as

$$[110]_{\text{LSAT}} // [110]_{\text{VO}_2 \text{ M1}} \\ (100)_{\text{LSAT}} // (002)_{\text{VO}_2 \text{ B}} \ \& \ (010)_{\text{LSAT}} // (\bar{2}02)_{\text{VO}_2 \text{ B}}$$

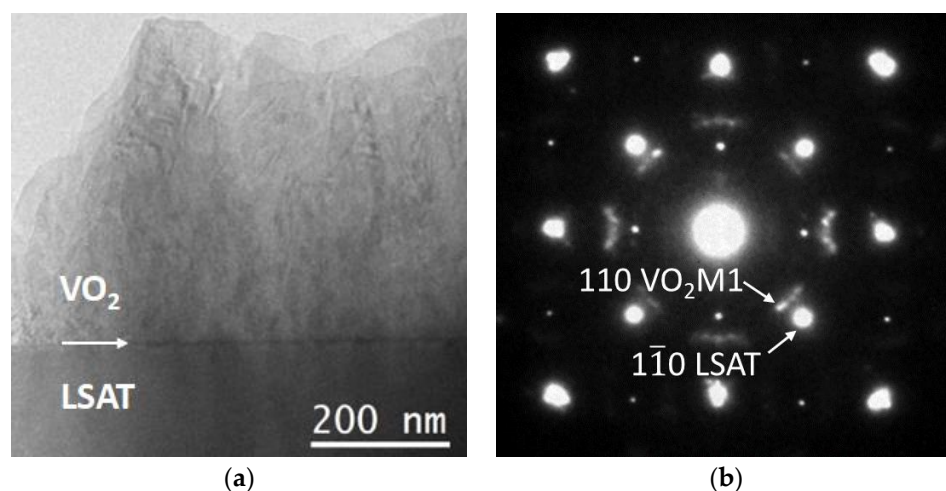


Figure 1. (a) TEM image of S1 VO₂ thin film on LSAT substrate, showing the general morphology; (b) SAD pattern from the interface area between VO₂ and the substrate.

Table 1. Structural parameters of the various VO₂ polymorphs found in the thin films.

VO ₂ Phase	Structure	Lattice Parameters
M1	Monoclinic	$a = 0.575$ nm $b = 0.454$ nm $c = 0.538$ nm $\beta = 122.6^\circ$
A	Tetragonal	$a = 0.844$ nm $c = 0.767$ nm
B	Monoclinic	$a = 0.121$ nm $b = 0.37$ nm $c = 0.643$ nm $\beta = 106.9^\circ$
R	Tetragonal	$a = 0.456$ nm $c = 0.286$ nm

The interfacial quality of VO₂/LSAT is depicted in more detail in the HRTEM images of Figure 2; a sharp and clear interface is illustrated, with minimum roughness. The VO₂ M1 phase is dominant in the film area, both at the exact interface, as well as in the upper regions of the VO₂ film, as demonstrated in Figure 2a. Moreover, the VO₂ M1 and LSAT (110) planes, marked in the HRTEM image in Figure 2b, are perfectly aligned, in full agreement with the SAD pattern analysis.

The structural mismatch between VO₂ and LSAT is expected to be accommodated for by the formation of misfit dislocation networks. The bright field (BF) image of Figure 3 illustrates a visualization of these misfit dislocations, as alternating dark and bright Moiré fringes, revealing the residual strain between the two lattices. The separation between the fringes, as measured both by BF images, as well as by satellite diffractions spots in common SAD patterns, was found to be $d_M = 1.94$ nm on average, in accordance with the mismatch between VO₂ M1 and LSAT.

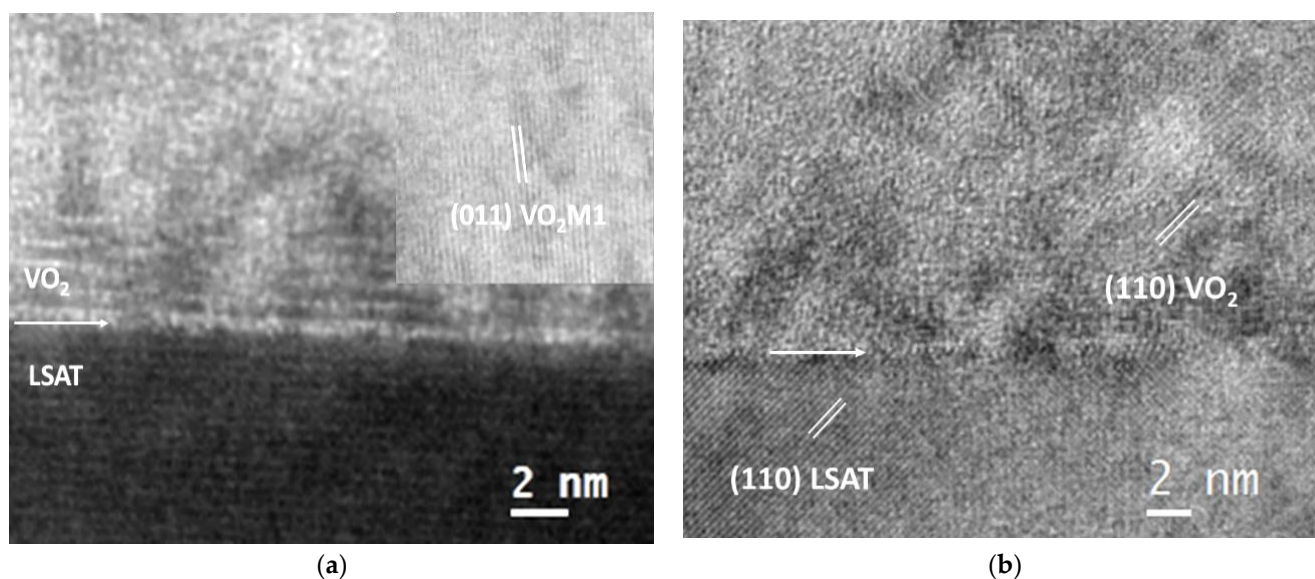


Figure 2. HRTEM images from the VO₂/LSAT interface showing the interfacial quality and the dominant VO₂ M1 phase.

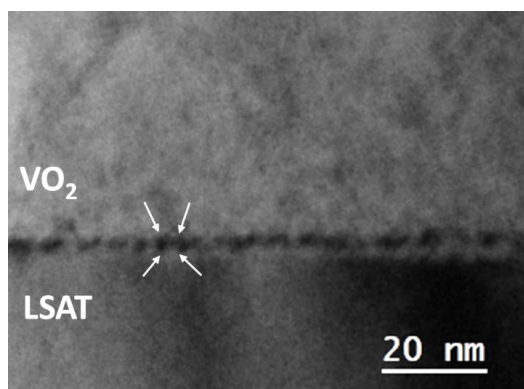


Figure 3. Cross-sectional image of the VO₂/LSAT interfacial area, viewed by the [001] LSAT zone axis.

The columnar morphology of the VO₂ thin films has been better illustrated by diffraction contrast-imaging experiments. In Figure 4, two typical complementary BF and dark field (DF) images of the VO₂/LSAT sample S1 are shown. The images were acquired using the $g = 002$ imaging vector of VO₂. The columnar morphology of the VO₂ area is apparent, with columns possessing typical widths of up to 170 nm towards the film's free surface region and heights of up to the total film thickness, i.e., 720 nm in this case. Moreover, the VO₂ columns have a high concentration of structural defects, which are mainly identified as twins, lying on {110} crystal planes. The SAD pattern of Figure 1b further confirms this observation.

The growth of VO₂ thin film on Si substrates revealed similar structural features. Figure 5 shows typical results from the TEM observations of a VO₂ film (S2) deposited with 20,000 pulses on Si (001). The VO₂ film in Figure 5a also exhibits a columnar mode of growth, with average column widths of about 35 nm. The total film thickness is up to 167 nm. For thicker VO₂ samples, i.e., S3 (50,000 pulses), where the total film thickness reaches 500 nm, the average column width proportionally increases to 93 nm in the film's free surface region. Inside such columns, a significant number of planar defects, such as extended twins have been observed, too, in agreement with the results from VO₂/LSAT. Figure 5b depicts a common SAD pattern of the film/substrate interfacial area. Si is oriented along its [011] zone axis, whereas reflections attributed to VO₂ reveal a multiplicity of phases. Here, the $\bar{2}02$ spots of the VO₂ B phase have been illustrated, for comparison.

Diffraction analysis revealed that the VO₂ films are polycrystalline, in full agreement with the films deposited on LSAT.

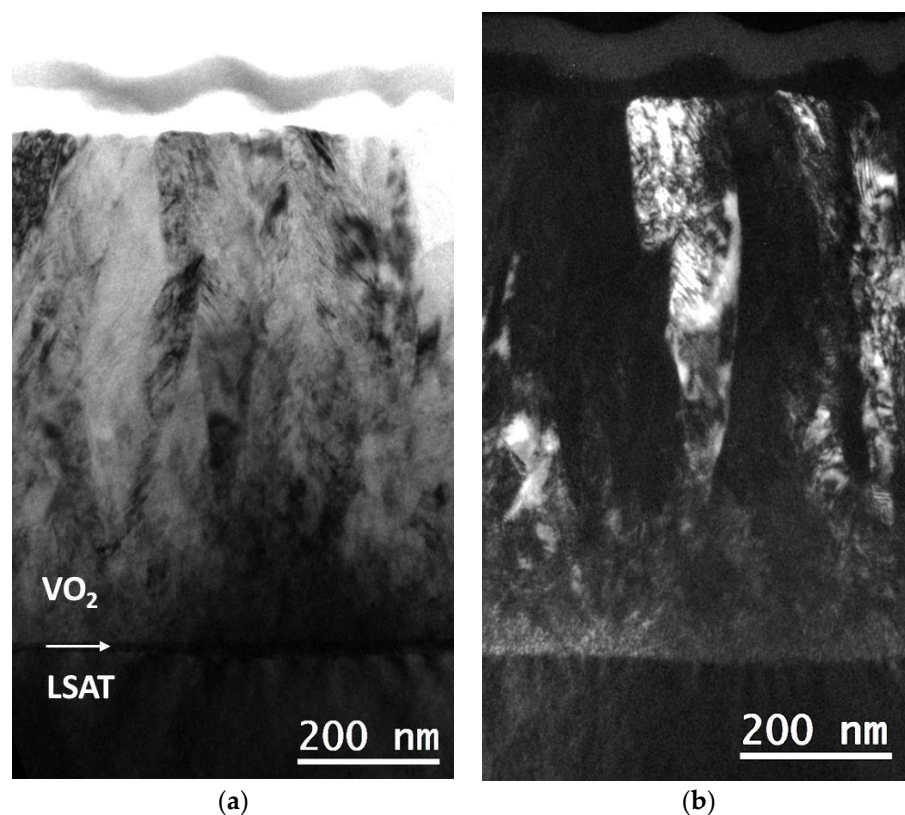


Figure 4. (a) BF image taken from S1 revealing the columnar growth of VO₂ thin film grown on LSAT; (b) complementary DF image from the same area, obtained with $g = 002$.

The HRTEM image in Figure 5c shows the VO₂/Si interfacial area in greater detail, where a smooth interface has been revealed. There is an approximately 2 nm thick intrinsic amorphous layer of SiO_x formed between the VO₂ film and the Si substrate [35]. Therefore, although an epitaxial relationship between the film and substrate is not feasible in this case [27], there are some VO₂ crystallites that aligned with or close to the main Si reflections, such as the VO₂ B ones, whose [101] direction is close to the Si [100] one.

The TEM analysis revealed the presence of several phases of VO₂, irrespective of the thickness of the film and the type of substrate. Despite the variation in the number of pulses and film thickness, the structural quality was found, in general, to be quite good.

Most interplanar d spacings corresponded to the monoclinic VO₂ (M1 type) but a good percentage of VO₂ B and VO₂ A phases were also found. Table 2 below summarizes the relative percentage of phases in the films, as estimated both by SAD pattern and HRTEM image analyses alike.

Table 2. Percentage of the dominant VO₂ phases detected in the thin films grown on LSAT and Si substrates.

Samples	VO ₂ M1	VO ₂ R	VO ₂ A	VO ₂ B
S1	54	11	6	29
S2	40	-	15	45
S3	53	-	12	35

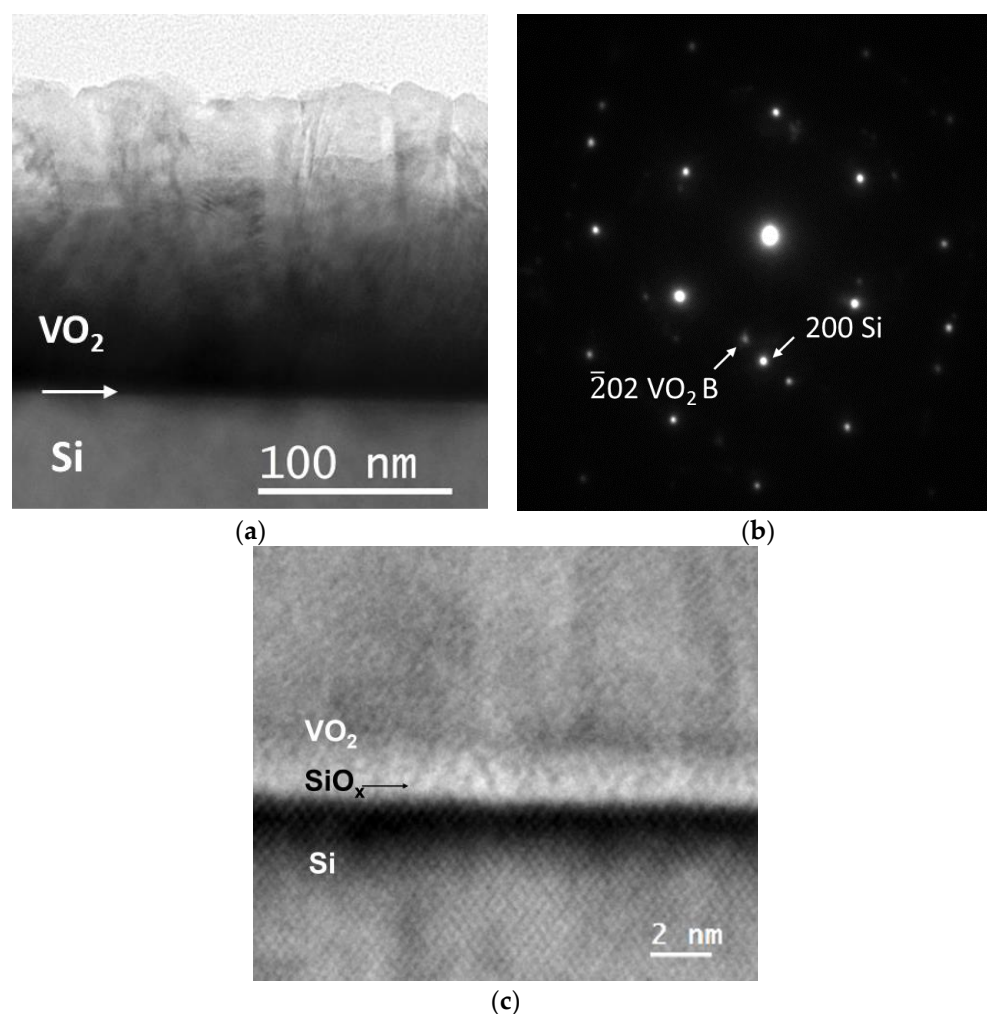


Figure 5. Microscopy results of the S2 VO₂ thin film on Si substrate: (a) conventional TEM image exhibiting columnar growth; (b) common SAD pattern taken from the interface area with Si being in the [011] zone axis; (c) HRTEM image of the VO₂/Si interfacial area showing its structural quality and the SiO_x intrinsic layer.

Post-experimental calculations of the residual strain present in the VO₂ films have been accomplished by applying the geometric phase analysis (GPA) method on HRTEM images [36]. Figure 6 summarizes the main outcomes from these calculations. In the case of the Si substrate in Figure 6a,b, the strain is negligible, as it is predominately released due to the SiO_x intrinsic amorphous layer formed between the substrate and film, along with the columnar VO₂ morphology [37]. On the other hand, the growth of VO₂ on top of LSAT as seen in Figure 6c,d is direct; however, the residual strain was still measured to be quite low and in the range of 5% on average, due to the columnar morphology of VO₂ crystallites [37]. Only locally, the residual strain reaches values of up to 8–10%, mainly at areas with defects present, as shown in Figure 6d. According to the lattice parameters of LSAT ($a = 0.387$ nm) and VO₂ M1 (Table 1) and their epitaxial relationship, the theoretical anticipated strain would be quite high, more than 17–20%; therefore, a great amount of strain relief is observed, due to the columnar morphology and polycrystalline nature of VO₂. In addition, the average strain along the c axis ($c_{\text{VO}_2} - c_{\text{LSAT}} / c_{\text{LSAT}}$) would still be high, equal to 39%. However, the GPA strain maps suggest that the strain distribution does not change significantly throughout the film thickness.

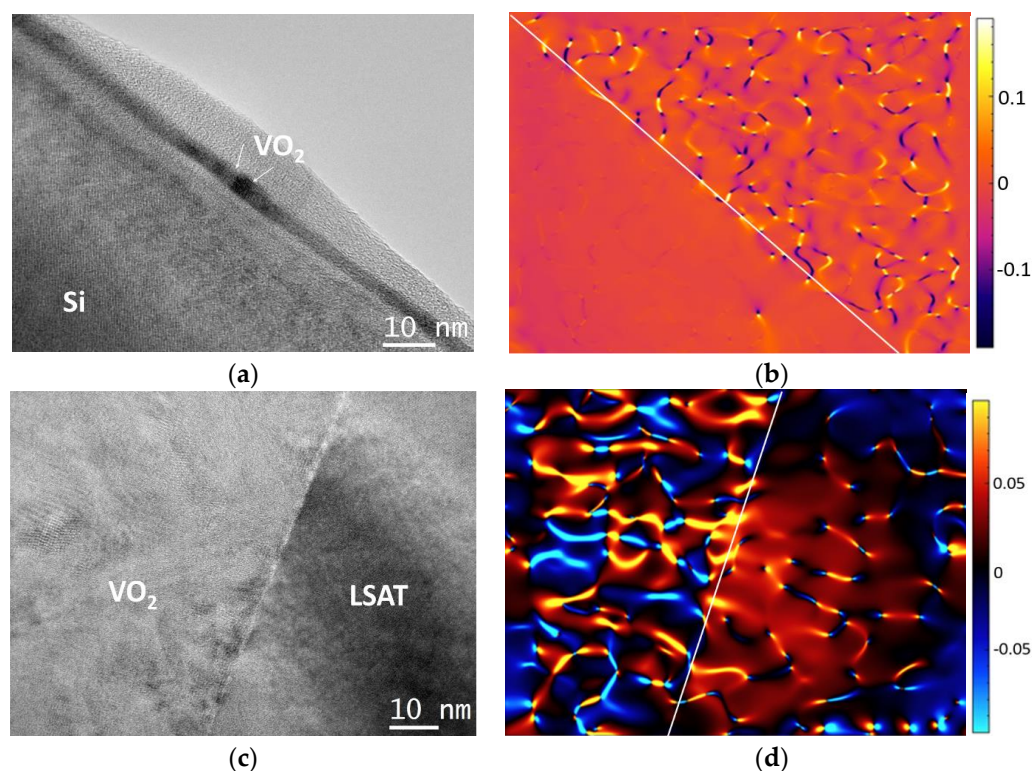


Figure 6. Typical GPA results from the VO₂ thin films: (a,c) HRTEM images; (b,d) corresponding GPA strain maps of VO₂/Si and VO₂/LSAT, respectively.

ΔA (resistance change), ΔT (sharpness), and ΔH (thermal hysteresis), and the reversibility of phase transition are all dependent on the quality of the film. Premkumar et al. reported a large variation in the resistance of films consisting of VO₂ M1 and VO₂ B phases at low temperature [38]. Considering the conduction behaviour, VO₂ M1 and VO₂ A are considered isolators (resistivities in the tens of Ohm.cm at room temperature, RT) and VO₂ B a semiconductor (resistivities in the order of 10^{-2} Ohm.cm at RT), whereas VO₂ R is considered to have a metallic character (resistivities in the order of 10^{-3} to 10^{-4} Ohm.cm at RT) [39]. However, a greater percentage of defects will lead to an increase in the resistivity of metallic VO₂ due to the enhanced scattering of electrons [32], whereas in the case of semiconducting VO₂, more energy levels are manifested in the band gap due to defects, leading to a resistivity decrease [40]. As a consequence, the resistivities of metallic and semiconducting films with various defects could become quite comparable at RT, and therefore the absolute values of the resistivities are not adequate to conclude an unambiguous attribution to the VO₂ B or VO₂ R phases. On the other hand, the MIT transition is usually assigned to a crystalline phase transformation from the higher temperature VO₂ R phase to the lower temperature VO₂ M1 phase at around 340 K, the transition being reversible and developing under a hysteretic character.

Temperature-dependent electron transport and magnetic measurements were performed under the assumption that any structural change would be reflected in both resistivity and magnetization behavior. The evolution of resistivity as a function of temperature for the thicker VO₂ films deposited on LSAT and Si substrates (S1 and S3 samples, respectively) is shown in Figure 7. A decrease in the resistivity by more than 20% is observed for sample S1, and by more than 100% for sample S3 in the temperature range from 280 to 340 K, where the transition from the VO₂ M1 to VO₂ R polymorph is expected. Moreover, these transitions are reversible and of a hysteretic type with a maximum hysteretic width of about 20 K, as specific to the above-mentioned MIT. However, these variations are far lower than the optimal variations of resistance/resistivity by about three orders of magnitude, as observed in a similar film of VO₂ deposited on a silica substrate at 600 °C, exemplified in

the lower inset of Figure 7. There, resistance values in the order of 10 Ohm, corresponding to values of 10^{-3} Ohm.cm for resistivity are reported in both cases, below and above the MIT. In comparison, the resistance in the case of the VO₂/silica at 600 °C is less than 10^{-1} Ohm above the MIT, resulting in a resistivity of about 10^{-5} Ohm.cm above 340 K, where a dominant R phase is expected. In this context, the much higher resistivity in the analyzed samples S1 and S3 at 340 K provides evidence for a dominant VO₂ B phase at such temperatures. This result is in line with the TEM analysis, showing a significant amount of the VO₂ B phase at RT, and gives support to the fact that only a low fraction of the initially present M1 phase was transformed into the R phase at the higher temperature, in both systems. That is, according to the resistivity data, the VO₂ B phase is still highly dominant over the newly formed R phase at higher temperatures.

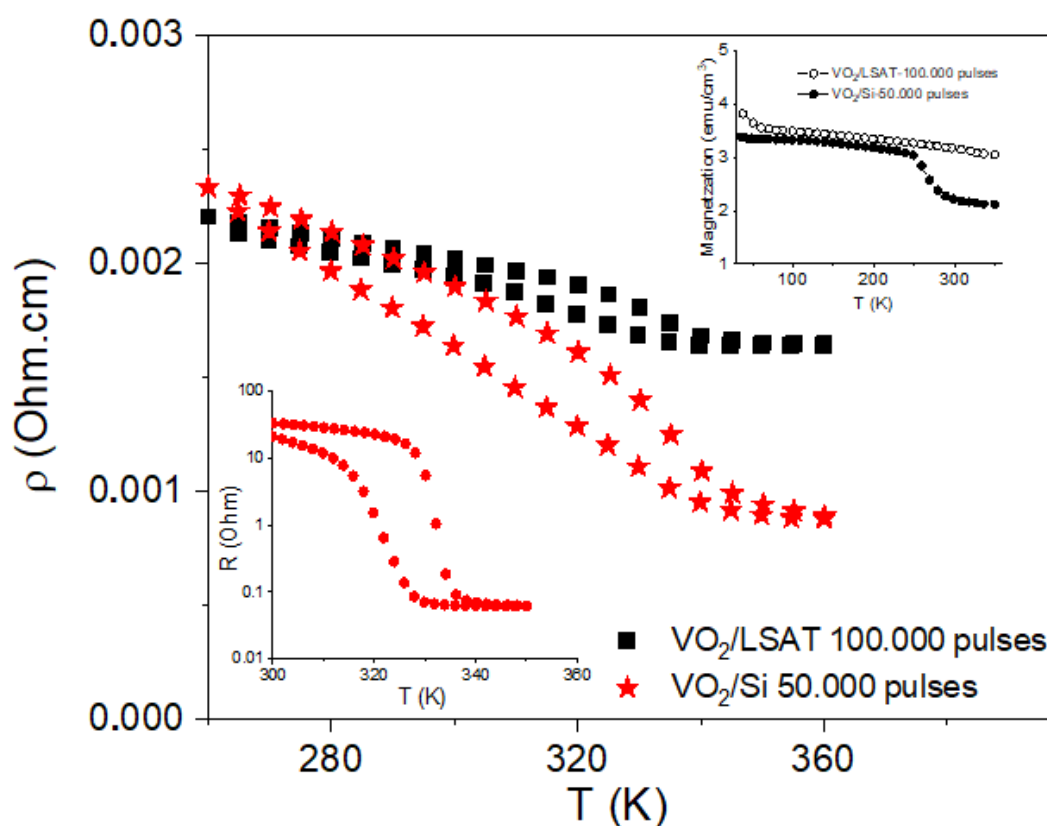


Figure 7. Temperature-dependent resistivity of S1 and S3 VO₂ films on LSAT and Si substrate, respectively. The upper inset shows the temperature-dependent magnetizations of the same films under a 300 Oe applied magnetic field, whereas the lower inset illustrates the temperature-dependent resistance of a similar VO₂ film, deposited on silica at 600 °C.

It is worth noticing from Table 2 that the initial content of the M1 phase was almost similar in both samples, whereas the resistivity of the S1 sample, already stabilizing 11% of the R phase, is higher than that of sample S3 at 340 K. This means that a higher fraction of the M1 phase has been transformed into the R phase in sample S3 as compared to S1. Tentatively, by the correlation of the resistivity results with the initial phase composition of the S1 and S3 films (see Table 2), it might be assumed that, for a more complete MIT, it is necessary to predominately avoid the formation of the VO₂ R and secondary to avoid the formation of the rather stable VO₂ B phases in the initial films (below the MIT).

The magnetic moments of the samples presented in the upper inset of the same figure are of the order of 10^{-5} emu (or a few emu/cm³ magnetization), which for such thin films, usually with oxygen vacancies, is specific to diluted magnetic oxide (DMO) behavior [41,42]. The different values and specific jumps in the magnetizations of the S1 and S3 films provide clear evidence for a different phase composition in the two films. For example, it is reported

in [43] that the susceptibility is almost constant with the temperature in the isolator M1 phase (order of magnitude of 10^{-6} emu/g/Oe, bulk sample) but increases by one order of magnitude in the metallic R phase. In the current thin films, the susceptibilities are in the range of 10^{-3} emu/g/Oe, showing that, due to many defects in thin films (usually associated to oxygen vacancies), the DMO character is prevailing for the analyzed samples and at the same time hinders the much lower change in susceptibility along MIT. This is also the reason that no increase in the magnetization above RT is observed, in direct relation to the M1 to R phase transformation, as reported in [43]. The tiny structural changes of % order from the M1 to R type phase in the present are, however, still observable by only the most sensitive changes in the resistivity (3–4 orders of magnitude over about 100% M1 to R phase change). On the other hand, a decrease in the magnetization (by some 30%) is observed in sample S3 at about 260 K. The easier conversion of the B phase to the unstable M1 and further into the R phase has been reported in many cases and expectedly the more conductive (semiconducting) B phase should have a higher magnetization than the M1 phase, as well as an increased number of oxygen vacancies, also responsible for an increased magnetization in DMO systems; thus, we may tentatively assume that the decrease in magnetization over 260 K is due to the transformation of the B phase into the M1 phase.

4. Conclusions

VO₂ thin films were successfully fabricated on LSAT and Si substrates using pulsed laser deposition with the aim of investigating the correlations between morpho-structural aspects, phase composition, and the related MIT transitions. Transmission electron microscopy techniques were used for a thorough structural investigation of the VO₂ thin films, whereas resistivity and magnetic measurements were considered for the investigation of the specifically involved temperature-driven phase transitions. The films exhibited columnar growth regardless of the substrate. HRTEM imaging and SAD pattern acquisition revealed nanoscale grains of different phases, namely VO₂ M1, VO₂ A, VO₂ B, and VO₂ R. The thickest films exhibited the VO₂ M1 phase as dominant (more than 50%) prior to the MIT transition but the VO₂ B type was also stabilized in high amounts. The residual strain was relieved, predominantly due to the columnar morphology, along with the SiO_x layer for the samples on Si substrates. In this context of very low residual strain, the less intense MITs in the thicker films were interpreted in terms of only a partial (a few %) M1 to R structural phase transition, specifically driven by the initial phase composition of the films. It was shown that the initial formation of the VO₂ R phase, as well as the presence of the VO₂ B phase, considerably diminishes both the sharpness and the resistance change in the VO₂ films. According to this study, the lack of residual strain may impede the structural M1 to R transformation, in spite of a consistent presence of the M1-type phase in the films at RT.

Author Contributions: Conceptualization, A.D.; formal analysis, A.R. and A.D.; funding acquisition, A.D.; investigation, A.R., N.I., A.L., C.L., V.K., C.N.M. and A.D.; methodology, A.D.; project administration, A.D.; resources, A.D.; supervision, A.D.; visualization, A.D.; writing—original draft, A.R., N.I., A.L. and C.L.; writing—review and editing, V.K., C.N.M., and A.D. All authors have read and agreed to the published version of the manuscript.

Funding: This research was funded by EEA/Norway grants—Norway–Romania Collaborative Research Projects 2019, grant number RO-NO-2019-0498 (TEESM project). The NIMP authors also acknowledge the Romanian Ministry of Research, Innovation, and Digitalization in the framework of Core Program PN19-03 (Contract No. 21 N/08.02.2019). The APC was funded by the University of Stavanger and MDPI.

Data Availability Statement: All data is available throughout the manuscript.

Conflicts of Interest: The authors declare no conflict of interest.

References

1. Zhou, Y.; Fan, F.; Liu, Y.; Zhao, S.; Xu, Q.; Wang, S.; Luo, D.; Long, Y. Unconventional smart windows: Materials, structures and designs. *Nano Energy* **2021**, *90*, 106613. [[CrossRef](#)]
2. Lombard, L.P.; Ortiz, J.; Pout, C. A review on buildings energy consumption information. *Energy Build.* **2008**, *40*, 394–398. [[CrossRef](#)]
3. Wang, M.; Xing, X.; Perepichka, I.F.; Shi, Y.; Zhou, D.; Wu, P.; Meng, H. Electrochromic smart windows can achieve an absolute private state through thermochromically engineered electrolyte. *Adv. Energy Mater.* **2019**, *9*, 1900433. [[CrossRef](#)]
4. Searchinger, T.D.; Beringer, T.; Holtzmark, B.; Kammen, D.M.; Lambin, E.F.; Lucht, W.; Raven, P.; Ypersele, J.P.V. Europe's renewable energy directive poised to harm global forests. *Nat. Commun.* **2018**, *9*, 3741. [[CrossRef](#)] [[PubMed](#)]
5. Shin, M.; Baltazar, J.C.; Haberl, J.S.; Frazier, E.; Lynn, B. Evaluation of the energy performance of a net zero energy building in a hot and humid climate. *Energy Build.* **2019**, *204*, 109531. [[CrossRef](#)]
6. Zhang, G.; Li, X.; Shi, W.; Wang, B.; Cao, Y. Influence of occupant behaviour on the energy performance of variable refrigerant flow systems for office buildings: A case study. *J. Build. Eng.* **2019**, *22*, 327–334. [[CrossRef](#)]
7. Granqvist, C.G. Recent progress in thermochromics and electrochromics: A brief survey. *Thin Solid Films* **2016**, *614*, 90–96. [[CrossRef](#)]
8. Llordes, A.; Garcia, G.; Gazquez, J.; Milliron, D.J. Tunable near-infrared and visible light transmittance in nanocrystal-in-glass composites. *Nature* **2013**, *500*, 323–326. [[CrossRef](#)]
9. Cai, G.; Wang, J.; Lee, P.S. Next-generation multifunctional electrochromic devices. *Acc. Chem. Res.* **2016**, *49*, 1469–1476. [[CrossRef](#)]
10. Ke, Y.; Zhou, C.; Zhou, Y.; Wang, S.; Chan, S.H.; Long, Y. Emerging thermal responsive materials and integrated techniques targeting the energy-efficient smart window application. *Adv. Funct. Mater.* **2018**, *28*, 1800113. [[CrossRef](#)]
11. Khandelwal, H.; Schenning, A.P.H.J.; Debije, M.G. Infrared regulating smart window based on organic materials. *Adv. Energy Mater.* **2017**, *7*, 1602209. [[CrossRef](#)]
12. Amasawa, E.; Sasagawa, N.; Kimura, M.; Taya, M. Design of a new energy harvesting electrochromic window based on an organic polymeric dye, a cobalt couple, and PProDOT-Me₂. *Adv. Energy Mater.* **2014**, *4*, 1400379. [[CrossRef](#)]
13. Mann, D.; Yeung, C.; Habets, R.; Vroon, Z.; Buskens, P. Comparative building energy simulation study of static and thermochromically adaptive energy-efficient glazing in various climate regions. *Energies* **2020**, *13*, 2842. [[CrossRef](#)]
14. Gagaoudakis, E.; Michail, G.; Aperathitis, E.; Kortidis, I.; Binas, V.; Panagopoulou, M.; Raptis, Y.S.; Tsoukalas, D.; Kiriakidis, G. Low temperature rf-sputtered thermochromic VO₂ films on flexible glass substrates. *Adv. Mater. Lett.* **2017**, *8*, 757–761. [[CrossRef](#)]
15. Granqvist, C.G. Electrochromics and thermochromics: Towards a new paradigm for energy efficient buildings. *Mater. Today Proc.* **2016**, *3*, S2–S11. [[CrossRef](#)]
16. Vernardou, D.; Pemble, M.E.; Sheel, D.W. In-situ FTIR studies of the growth of vanadium dioxide coatings on glass by atmospheric pressure chemical vapour deposition for VCl₄ and H₂O system. *Thin Solid Film.* **2007**, *515*, 8768–8770. [[CrossRef](#)]
17. Koo, H.; You, H.W.; Ko, K.E.; Kwon, O.J.; Chang, S.H.; Parka, C. Thermochromic properties of VO₂ thin film on SiNx buffered glass substrate. *Appl. Surf. Sci.* **2013**, *277*, 237–241. [[CrossRef](#)]
18. Pouget, J.P.; Launois, H.; D'Haenens, J.P.; Merenda, P.; Rice, T.M. Electron Localization Induced by Uniaxial Stress in Pure VO₂. *Phys. Rev. Lett.* **1975**, *13*, 35. [[CrossRef](#)]
19. Narayan, J.; Bhosle, V.M. Phase transition and critical issues in structure-property correlations of vanadium oxide. *J. Appl. Phys.* **2006**, *100*, 103524. [[CrossRef](#)]
20. Bayati, M.R.; Molaei, R.; Wub, F.; Budai, J.D.; Liu, Y.; Narayan, R.J.; Narayan, J. Correlation between structure and semiconductor-to-metal transition characteristics of VO₂/TiO₂/sapphire thin film heterostructures. *Acta Mater.* **2013**, *61*, 7805–7815. [[CrossRef](#)]
21. Burkhardt, W.; Christmann, T.; Franke, S.; Kriegseis, W.; Meister, D.; Meyer, B.K. Tungsten and fluorine co-doping of VO₂ films. *Thin Solid Films* **2002**, *402*, 226. [[CrossRef](#)]
22. Ruzmetov, D.; Ramanathan, S. *Thin Film Metal Oxides: Fundamentals and Applications in Electronics and Energy*; Springer: New York, NY, USA, 2010.
23. Choi, Y.; Jung, Y.; Kim, H. Low-temperature deposition of thermochromic VO₂ thin films on glass substrates. *Thin Solid Films.* **2016**, *615*, 437–445. [[CrossRef](#)]
24. Kolenatý, D.; Vlček, J.; Bárta, T.; Rezek, J.; Houška, J.; Haviar, S. High-performance thermochromic VO₂-based coatings with a low transition temperature deposited on glass by a scalable technique. *Sci. Rep.* **2020**, *10*, 11107. [[CrossRef](#)]
25. Malarde, D.; Powell, M.J.; Quesada-Cabrera, R.; Wilson, R.L.; Carmalt, C.J.; Sankar, G.; Parkin, I.P.; Palgrave, R.G. Optimized Atmospheric-Pressure Chemical Vapor Deposition Thermochromic VO₂ Thin Films for Intelligent Window Applications. *ACS Omega* **2017**, *2*, 1040–1046. [[CrossRef](#)]
26. Li, D.; Li, M.; Pan, J.; Luo, Y.; Wu, H.; Zhang, Y.; Li, G. Hydrothermal Synthesis of Mo-Doped VO₂/TiO₂ Composite Nanocrystals with Enhanced Thermochromic Performance. *Appl. Mater. Interfaces* **2014**, *6*, 6555–6561. [[CrossRef](#)]
27. Manning, T.D.; Parkin, I.P. Vanadium(IV) oxide thin films on glass and silicon from the atmospheric pressure chemical vapour deposition reaction of VOCl₃ and water. *Polyhedron* **2004**, *23*, 3087–3095. [[CrossRef](#)]
28. Chang, T.; Cao, X.; Li, N.; Long, S.; Gao, X.; Dedon, L.R.; Sun, G.; Luo, H.; Jin, P. Facile and Low-Temperature Fabrication of Thermochromic Cr₂O₃/VO₂ Smart Coatings: Enhanced Solar Modulation Ability, High Luminous Transmittance and UV-Shielding Function. *Appl. Mater. Interfaces* **2017**, *9*, 26029–26037. [[CrossRef](#)]
29. Kim, D.H.; Kwok, H.S. Pulsed laser deposition of VO₂ thin films. *Appl. Phys. Lett.* **1994**, *65*, 3188. [[CrossRef](#)]

30. Chang, T.; Zhu, Y.; Huang, J.; Luo, H.; Jin, P.; Cao, X. Flexible VO₂ thermochromic films with narrow hysteresis loops. *Sol. Energy Mater. Sol. Cells* **2021**, *219*, 110799. [[CrossRef](#)]
31. Kim, C.Y.; Kim, S.H.; Kim, S.J.; An, K.S. VO₂ (110) film formation on TiO₂(110) through post-reduction of ALD grown vanadium oxide. *Appl. Surf. Sci.* **2014**, *313*, 368–371. [[CrossRef](#)]
32. Jian, J.; Chen, A.; Zhang, W.; Wang, H. Sharp semiconductor-to-metal transition of VO₂ thin films on glass substrates. *J. Appl. Phys.* **2013**, *114*, 244301. [[CrossRef](#)]
33. Jian, J.; Chen, A.; Chen, Y.; Zhang, X.; Wang, H. Roles of strain and domain boundaries on the phase transition stability of VO₂ thin films. *Appl. Phys. Lett.* **2017**, *111*, 153102. [[CrossRef](#)]
34. Yamagushi, I.; Manabe, T.; Tsyuchia, T.; Nakajima, T.; Sohma, M.; Kumagai, T. Preparation and Characterization of Epitaxial VO₂ Films on Sapphire Using Postepitaxial Topotaxy Route via Epitaxial V₂O₃ Films. *Jpn. J. Appl. Phys.* **2008**, *47*, 1022. [[CrossRef](#)]
35. Goodnick, S.M.; Fathipour, M.; Ellsworth, D.L.; Wilmsen, C.W. Effects of a thin SiO₂ layer on the formation of metal–silicon contacts. *J. Vac. Sci. Technol.* **1981**, *18*, 949. [[CrossRef](#)]
36. Hýtch, M.J.; Snoek, E.; Kilaas, R. Quantitative measurement of displacement and strain fields from HREM micrographs. *Ultramicroscopy* **1998**, *74*, 131. [[CrossRef](#)]
37. Kehagias, T.; Delimitis, A.; Kominou, P.; Iliopoulos, E.; Dimakis, E.; Georgakilas, A.; Nouet, G. Misfit accommodation of compact and columnar InN epilayers grown on Ga-face GaN (0001) by molecular-beam epitaxy. *Appl. Phys. Lett.* **2005**, *86*, 151905. [[CrossRef](#)]
38. Premkumar, P.A.; Toeller, M.; Radu, J.P.; Adelman, C.; Schaeckers, M.; Meersschaut, J.; Conard, T.; Elshochta, S.V. Process Study and Characterization of VO₂ Thin Films Synthesized by ALD Using TEMAV and O₃ Precursors. *ECS J. Solid State Sci. Technol.* **2012**, *1*, P169–P174. [[CrossRef](#)]
39. Lee, S.; Ivanov, I.N.; Keum, J.K.; Lee, H.N. Epitaxial stabilization and phase instability of VO₂ polymorphs. *Sci. Rep.* **2016**, *6*, 19621. [[CrossRef](#)] [[PubMed](#)]
40. Brassard, D.; Fourmaux, S.; Jean-Jacques, M.; Kieffer, J.C.; El Khakani, M.A. Grain size effect on the semiconductor-metal phase transition characteristics of magnetron-sputtered VO₂ thin films. *Appl. Phys. Lett.* **2005**, *87*, 051910. [[CrossRef](#)]
41. Tolea, F.; Sorescu, M.; Diamandescu, L.; Iacob, N.; Tolea, M.; Kuncser, V. Unidirectional Magnetic Anisotropy in Molybdenum Dioxide–Hematite Mixed-Oxide Nanostructures. *Nanomaterials* **2022**, *12*, 938. [[CrossRef](#)] [[PubMed](#)]
42. Tolea, F.; Grecu, M.N.; Kuncser, V.; Constantinescu, S.G.; Ghica, D. On the role of Fe ions on magnetic properties of doped TiO₂ nanoparticles. *Appl. Phys. Lett.* **2015**, *106*, 142404. [[CrossRef](#)]
43. Zhang, R.; Fu, Q.S.; Yin, C.Y.; Li, C.L.; Chen, X.H.; Qian, G.Y.; Lu, C.L.; Yuan, S.L.; Zhao, X.J.; Tao, H.Z. Understanding of metal-insulator transition in VO₂ based on experimental and theoretical investigations of magnetic features. *Sci. Rep.* **2018**, *8*, 17093. [[CrossRef](#)] [[PubMed](#)]